NANO LETTERS

Letter

pubs.acs.org/NanoLett

# Templating Sub-10 nm Atomic Layer Deposited Oxide Nanostructures on Graphene via One-Dimensional Organic Self-Assembled Monolayers

Justice M. P. Alaboson,[†,‡] Chun-Hong Sham,[†] Sumit Kewalramani,[†] Jonathan D. Emery,[†] James E. Johns,[†] Aparna Deshpande,[†,#] TeYu Chien,[†] Michael J. Bedzyk,[†,§] Jeffrey W. Elam,[⊥] Michael J. Pellin,[‡,∥] and Mark C. Hersam[†,∥,○,*]

[†]Department of Materials Science and Engineering, Northwestern University, 2220 Campus Drive, Evanston, Illinois 60208, United States

[‡]Materials Science Division, Argonne National Laboratory, Argonne, Illinois 60439, United States

[§]Department of Physics and Astronomy, Northwestern University, Evanston, Illinois 60208, United States

[⊥]Energy Systems Division, Argonne National Laboratory, Argonne, Illinois 60439, United States

[∥]Department of Chemistry, Northwestern University, Evanston, Illinois 60208, United States

[○]Department of Medicine, Northwestern University, Evanston, Illinois 60208, United States

Supporting Information

**ABSTRACT:** Molecular-scale control over the integration of disparate materials on graphene is a critical step in the development of graphene-based electronics and sensors. Here, we report that self-assembled monolayers of 10,12-pentacosadiynoic acid (PCDA) on epitaxial graphene can be used to template the reaction and directed growth of atomic layer deposited (ALD) oxide nanostructures with sub-10 nm lateral resolution. PCDA spontaneously assembles into well-ordered domains consisting of one-dimensional molecular chains that coat the entire graphene surface in a manner consistent with the symmetry of the underlying graphene lattice. Subsequently, zinc oxide and alumina ALD precursors are shown to preferentially react with the functional moieties of PCDA, resulting in templated oxide nanostructures. The retention of the original one-dimensional molecular ordering following ALD is dependent on the chemical reaction pathway and the stability of the monolayer, which can be enhanced via ultraviolet-induced molecular cross-linking.

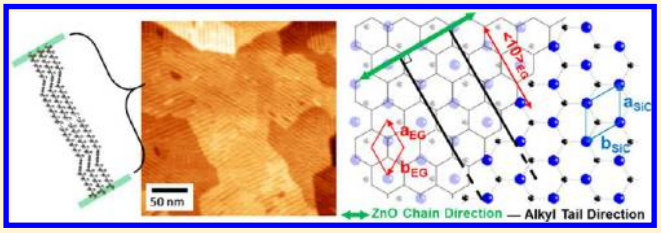


**KEYWORDS:** *Epitaxial graphene, silicon carbide, pentacosadiynoic acid, ALD, zinc oxide, alumina*

The superlative electronic properties of graphene, particularly its high charge carrier mobility,[1,2] make it a promising material for many applications in electronics,[3−5] photonics,[6] sensing,[7] and energy technologies.[8] However, despite its intrinsic potential, the chemical inertness of the basal plane of graphene poses serious challenges for its integration with complementary electronic materials such as high-*k* dielectrics.[9] Furthermore, the absence of a bandgap in pristine graphene limits its applicability for high-value targets such as digital electronics, thus motivating efforts to tailor the bandstructure of graphene via chemical templating at the sub-10 nm scale.[10,11] While bulk chemical functionalization schemes for graphene have begun to emerge,[12−16] the desired molecular-level control over macroscopic areas remains elusive.

Early attempts at materials integration with graphene have largely focused on the incorporation of atomic layer deposited (ALD) high-*k* dielectrics for graphene-based field-effect transistor applications. To improve the coverage and uniformity of ALD films, the inert graphene surface requires pretreatment with ozone,[17,18] nitrogen dioxide,[5] oxidized metal films,[19,20] spin-coated polymer films,[3] or organic self-assembled monolayers.[14,21] Meanwhile, the majority of other graphene chemical functionalization methods have been used to facilitate solution-phase processing of graphene[22−25] or the formation of graphene-polymer composites.[26−29] Recent work has shown that many of these chemical modification schemes can be controlled down to the nanometer-scale, although such work has been limited to localized serial nanopatterning with limited scalability to large areas.[30−32]

In contrast, noncovalent self-assembled organic monolayers can achieve wafer-scale functionalization of graphene, with low-defect density domains that span hundreds of nanometers.[15,33,34] The resulting molecular-level structure of these self-assembled monolayers is guided by hydrogen bonding between molecular functional groups and noncovalent

**Received:** January 9, 2013
**Revised:** February 28, 2013

   dx.doi.org/10.1021/nl4000932 | *Nano Lett.* XXXX, XXX, XXX−XXX

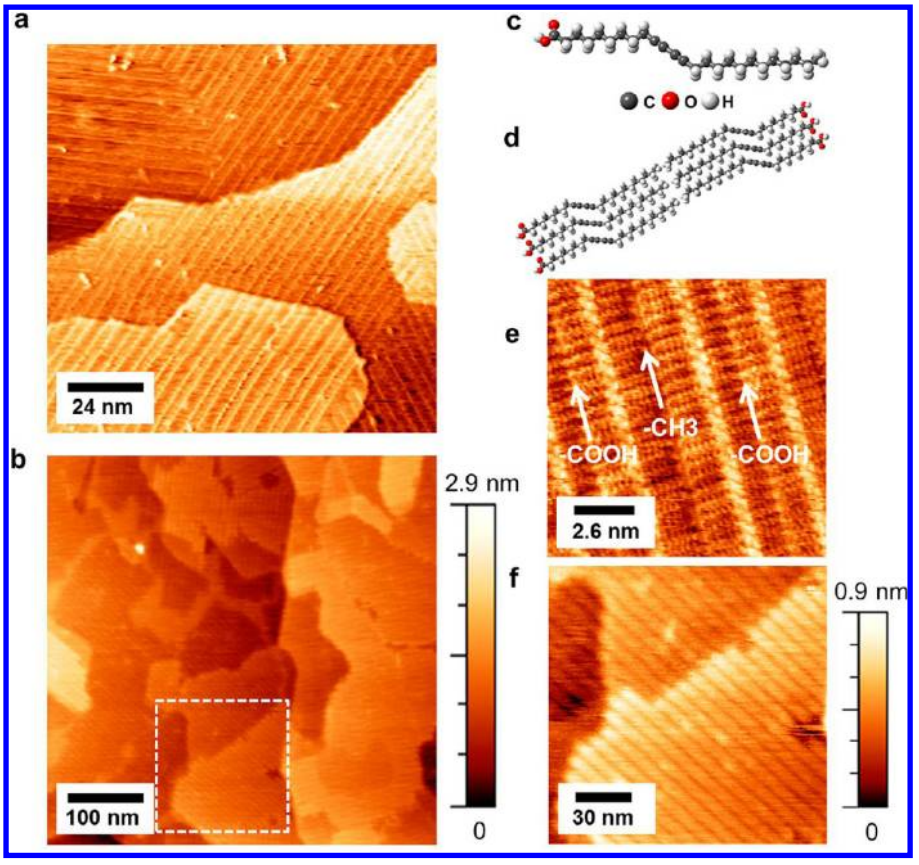


**Figure 1.** Self-assembled monolayer of 10,12-pentacosadiynoic acid (PCDA) on epitaxial graphene (EG). (a) UHV STM image of PCDA on epitaxial graphene (EG). PCDA self-assembles into monolayer domains consisting of 1D stripes on the graphene surface. (b) AFM image of a PCDA/EG surface in ambient conditions, showing the 1D molecular arrays. (c) Molecular structure of 10,12-pentacosadiynoic acid (PCDA). (d) Schematic of the molecular assembly of PCDA. (e) Molecularly resolved UHV STM image of PCDA/EG. The bright protrusions are the diacetylene groups, while the terminal ends of the molecule are indicated in the figure. (f) Zoomed-in AFM image of part b. The periodicity of the stripes in AFM corresponds to the length of two PCDA molecules.

interactions with the underlying graphene layer. While reports exist of using such self-assembled systems for nanostructuring graphene,[16,33,35−37] these patterning strategies are often based on nanospheres or block copolymers, which are substantially larger than small organic molecules. Furthermore, functional groups incorporated in the constituent organic molecules of self-assembled systems have rarely been utilized to enable tailored reactivity or to direct subsequent chemistry on graphene.

Here, we demonstrate that self-assembled monolayers of 10,12-pentacosadiynoic acid (PCDA) on epitaxial graphene (EG) can be used to template the reaction and directed growth of atomic layer deposited (ALD) films with sub-10 nm lateral resolution. PCDA is deposited via sublimation in ultrahigh vacuum (UHV) and is shown to self-assemble into well-ordered monolayer domains consisting of one-dimensional (1D) molecular nanostructures that coat the surface in a manner consistent with the symmetry of the underlying graphene lattice. Typical ALD chemistries for the growth of ZnO and $Al_2O_3$ are investigated on these PCDA/EG templates. The results show that ALD precursors preferentially react with the molecular functional groups of PCDA, and these reactions can be either self-terminating, with limited vertical growth, or nonterminating, where film growth is observed as a function of ALD cycle number. The retention of the one-dimensional molecular-scale ordering on the PCDA template following ALD depends on the chemical details of the precursor-molecular functional group interactions, as well as the overall stability of the PCDA monolayer, the latter of which can be enhanced via ultraviolet-induced cross-linking. Furthermore, selected ALD chemistries also prove to stabilize the PCDA monolayer, which subsequently produce larger domain sizes upon annealing. Overall, the combination of PCDA and ALD provide multiple pathways for the formation of sub-10 nm oxide nanostructures on graphene.

The epitaxial graphene (EG) samples were grown on n-type (nitrogen doped) 6H-SiC (0001) wafers (Cree, Inc.) by UHV graphitization.[14,15,31] Following *in situ* scanning tunneling microscopy (STM) confirmation of successful graphene growth, PCDA monolayers were formed on the graphene surface by sublimating PCDA (≥97%, Sigma Aldrich) from alumina-coated tungsten boats at room temperature in UHV. PCDA self-assembles into well-ordered monolayer domains consisting of one-dimensional molecular arrays that coat the entire graphene surface, as shown in the STM image of Figure 1a. The molecular structure and assembly of PCDA on graphene are presented schematically in Figure 1, parts c and d, respectively. The molecular domains are also seen to seamlessly span the atomic steps of the underlying EG/SiC substrate. In the molecularly resolved STM image (Figure 1e), the bright protrusions consist of the central diacetylene moieties of PCDA, while the terminal carboxylic and methyl ends are indicated with arrows.[38] The PCDA monolayer is primarily stabilized by hydrogen bonding between the carboxylate groups


dx.doi.org/10.1021/nl4000932 | *Nano Lett.* XXXX, XXX, XXX−XXX

of adjacent molecules and $\pi-\pi$ interactions between the diacetylene groups of neighboring molecules and the graphene surface. Hence, both the carboxylate and diacetylene moieties are responsible for self-assembly and important to overall monolayer stability, while also serving as possible sites for ALD precursor interactions. Consequently, the result of ALD on PCDA/EG templates depends on the details of the ALD reaction.

Representative ambient atomic force microscopy (AFM) images of the UHV-deposited PCDA samples are shown in Figure 1, parts b and f, thus confirming that the well-ordered stripes on the graphene surface are preserved following removal from the UHV environment. The distance between adjacent stripes was measured to be 7.3 ± 0.3 nm, which is attributed to the two-molecule terminal group periodicity of the monolayer,[38,39] with some reports assigning the center of the protrusions to the terminal carboxylate groups of PCDA.[39] The orientations of the PCDA domains are effectively 6-fold symmetric, oriented ~60° and 120° with respect to each other.[38] A similar ordering is also observed on HOPG and $MoS_2$ substrates, which have basal planes with hexagonal symmetry similar to that of graphene.[40,41]

Atomic layer deposition (ALD) was performed in a Savannah S100 ALD reactor (Cambridge Nanotech, Cambridge MA). For ALD of ZnO, the substrates were exposed to sequential doses of diethyl zinc (DEZ) and deionized water, with a purge step between each precursor dose. Figure 2a is an AFM topography image of the PCDA/EG sample after 15 cycles of ALD ZnO showing retention of the 6-fold ordering. X-ray photoelectron spectroscopy (XPS) was used to verify the presence of Zn on the sample surface following ALD. The acquired spectra were calibrated relative to the graphene C 1s peak at 285 eV. Figure 2b shows an XPS survey spectrum of the PCDA/EG sample after 15 cycles of ZnO ALD, with the Zn 2p peaks highlighted. The binding energy position of ~1022.6 eV for the Zn $2p_{3/2}$ peak (inset) is attributed to the presence of Zn−O. Other peaks in the survey scan are attributed to silicon, carbon, and oxygen, as expected for ZnO on EG/SiC.

After verification of the presence of ZnO with XPS, the absolute coverage of Zn was determined using X-ray fluorescence (XRF). Figure 2c shows the XRF-derived Zn coverage as a function of ALD cycles for $SiO_2$/Si and PCDA/EG/SiC substrates. The Zn coverage on the PCDA/EG surface is constant through the range of 5−60 ALD deposition cycles. Exposure of a PCDA/EG substrate to 15 pulses of the DEZ precursor alone, which is still effectively one ALD half-cycle, yielded identical XRF saturation coverage, suggesting that the DEZ precursor reaction with PCDA is self-terminating and the second ALD half-cycle reaction with $H_2O$ does not occur. By contrast, ALD growth on the $SiO_2$/Si surface progresses linearly, as is typical of nonterminating ALD processes.[42,43] The growth rate on $SiO_2$/Si is calculated to be 5.2 ± 0.3 (Zn/nm$^2$)/cycle, while the Zn coverage on PCDA/EG terminates at 1.2 ± 0.3 Zn/nm$^2$.

While limited in vertical growth, the modification of PCDA/EG with DEZ (ZnO−PCDA/EG) is sufficient to enhance its thermal stability. Figure S1 (Supporting Information) shows that while as-deposited PCDA completely desorbs at 110 °C under a pressure of 0.2 Torr, the ZnO-PCDA/EG substrates remain thermally stable under identical conditions, as verified by the persistence of the stripes. Furthermore, DEZ-modified PCDA/EG promotes enhanced ordering as the maximum domain size increases by a factor of 4 compared to unmodified

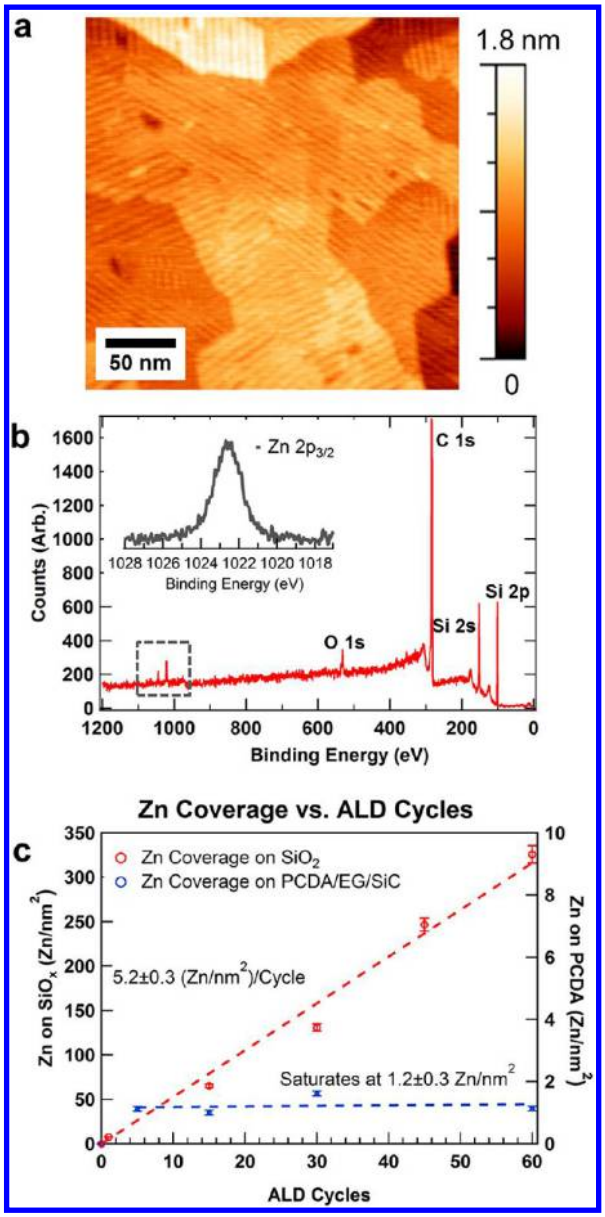


**Figure 2.** ALD of ZnO on PCDA/EG. (a) AFM image of PCDA/EG after 15 cycles of ALD ZnO using diethyl zinc (DEZ) and $H_2O$ as precursors. (b) A survey XPS spectrum of PCDA/EG after ZnO ALD showing the presence of Zn. (inset) The Zn $2p_{3/2}$ peak position is at ~1022.6 eV, indicating a Zn−O bond. The spectra were calibrated with respect to the C 1s peak at ~285 eV. (c) XRF Zn coverages as a function of ALD cycles for $SiO_2$/Si and PCDA/EG substrates. On $SiO_2$/Si, a linear increase in the coverage of Zn is observed, with a growth rate of 5.2 ± 0.3 (Zn/nm$^2$)/cycle. On the other hand, the Zn coverage terminates at 1.2 ± 0.3 Zn/nm$^2$ on the PCDA/EG substrate.

PCDA/EG following annealing (Figure S2). Similar crystallization into large domains has also been observed for molecules of phosphonic acids on HOPG.[44]

The self-terminating reaction of DEZ with PCDA and its improved thermal stability suggest that the Zn precursor is reacting uniformly with the PCDA/EG template. To gain further insight into the mechanism of ZnO ALD on PCDA/EG/SiC, we performed grazing-incidence small/wide-angle X-ray scattering (GISAXS/GIWAXS), which allows for the precise determination of the spatial distribution and orientation of the ZnO chains with respect to the underlying lattice. The


dx.doi.org/10.1021/nl4000932 | Nano Lett. XXXX, XXX, XXX−XXX

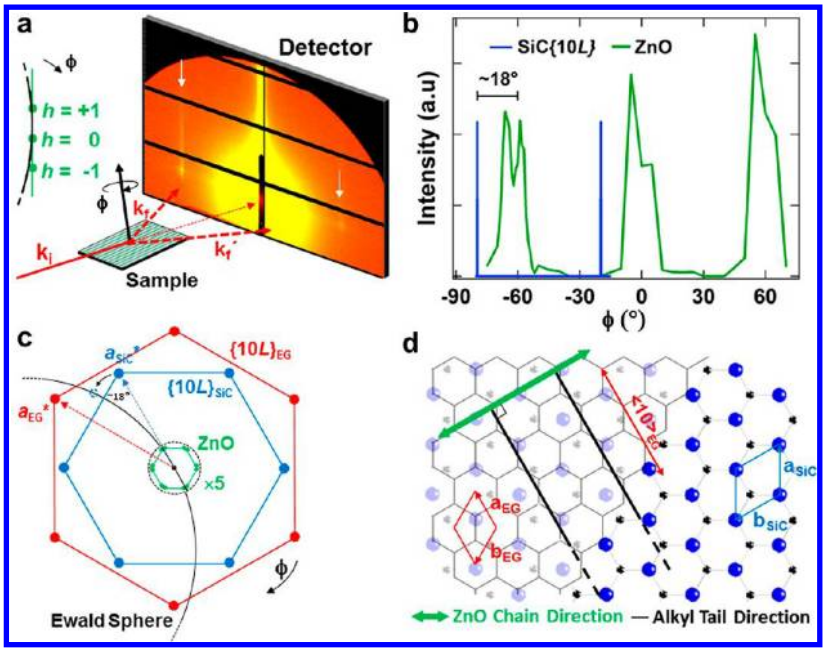


**Figure 3.** Grazing incidence small/wide-angle X-ray scattering. (a) Schematic of the GISAXS measurements on ZnO-PCDA/EG showing a GISAXS pattern near a ZnO 1D crystal Bragg condition. The $h = \pm 1$ Bragg conditions for ZnO at $q_y = \pm 0.96$ nm$^{-1}$ (indicated with white arrows) are satisfied at slightly different sample azimuthal angles, $\phi$, as illustrated with the Ewald sphere construction (for clarity, the reciprocal lattice is scaled by 5× as compared to the Ewald sphere radius). (b) Measured $\phi$ angular dependence of the near in-plane integrated intensities for the GISAXS ZnO rods (green line), and GIWAXS SiC{1 0 $L$} rods (blue line). (c) Reciprocal-space representation showing the relative positions of the ZnO (green), SiC (blue), and EG (red) rods projected onto the $L = 0$ $hk$ plane in accordance with the measurements in part b. The region inside the dashed circle has been scaled by 5× for clarity. A 1D ZnO reciprocal lattice from a single domain corresponds to two first order rods ($h = \pm 1$) separated by 180° in $\phi$, which are found to lie along the $\boldsymbol{a}_{SiC}$* reciprocal lattice vector. These are observed in part b to be split into two domains separated by 7°, which, due to the three domain orientations, produce a total of 12 rods. (d) A diagram of the real-space structure corresponding to the results in parts b and c, with EG and SiC in-plane unit cells in red and blue, respectively. The nominal ZnO chain direction is shown in green, and the alkyl chains lie along the EG ⟨1 0⟩ directions. The alkyl chains extend beyond the limits of the diagram.

experimental geometry is shown in Figure 3a (see Supporting Information for further details). The GISAXS and GIWAXS data are collected as a function of $q_y$ and $q_z$, which are the in-plane and the out-of-plane components of the scattering vector $\boldsymbol{q} = \boldsymbol{k}_f - \boldsymbol{k}_i$, where $\boldsymbol{k}_i$ and $\boldsymbol{k}_f$ are the incoming and outgoing X-ray wave vectors.

Figure 3a shows a 2D GISAXS pattern for ZnO-PCDA/EG in which two first-order $q_z$-extended Bragg rods at $q_y = \pm 0.96$ nm$^{-1}$ are observed (as indicated in the figure by white arrows). These peaks are not observed prior to ZnO ALD (see Figure S3a, Supporting Information.) The difference in the observed intensities of these rods depends on the azimuthal orientation of the sample, which determines the intersection of the Ewald sphere with the rods at $h = \pm 1$ of the ZnO reciprocal lattice, also shown in Figure 3a. Lorentzian fits to the $q_z$-integrated intensity for these rods reveal a 1D periodicity of $d = 2\pi/|q_y| = 6.57 \pm 0.04$ nm between the ZnO chains and a correlation length $L \sim 2\pi/\delta q_y \sim 100$ nm ($\delta q_y$ is the FWHM for the Bragg rods in the intensity profile). These values are consistent with the AFM-derived domain size and two-molecule periodicity, which indicates a coherent coupling between the Zn and the PCDA positions that is commensurate with the two-molecule periodicity of PCDA. The above GISAXS results, together with the verification of the presence of Zn−O from XPS, indicate that the carboxylate groups are the host sites for Zn atoms on PCDA/EG.

The orientational relationship between the ZnO-PCDA and the underlying EG lattice can be quantified by directly measuring the near in-plane scattered intensity for the ZnO first-order rods and the SiC{1 0 $L$} family of rods as a function of azimuthal angle, $\phi$. The integrated intensities from sequentially collected GISAXS ZnO and GIWAXS SiC signals are shown on the same $\phi$−scale in Figure 3b. An intensity map showing $q_y$-projected scattering patterns as a function of $\phi$ is shown in Figure S3b, Supporting Information. As discussed above, the diffraction peaks at $q_y = \pm 0.96$ nm$^{-1}$ arise from the periodic distribution of Zn coupled with the PCDA carboxylate headgroups, which implies that the PCDA alkyl chain will be oriented approximately normal[38] to the one-dimensional ZnO nanostructures. As seen in Figure 3b, intensity doublets (maxima separated by 7°) are observed at 60° intervals in $\phi$, confirming the effective 6-fold symmetry of ZnO-PCDA on EG/SiC, as is consistent with the AFM images in Figure 2a. The 7° separated doublet feature is consistent with observations of misoriented PCDA domains observed in STM (see Supporting Information for further details).[38,41] Hexagonal symmetry is also evident for the SiC{1 0 $L$ } family of rods, for which the scattered intensity is maximized at an angular offset of $\Delta\phi = -18 \pm 0.5°$ with respect to the ZnO rods.

The $L = 0$ cut for the reciprocal space lattices of the ZnO-PCDA/EG/SiC structure, shown in Figure 3c, depicts the Ewald sphere passing through the center of the $h = 1$ ZnO doublet and therefore exciting that Bragg condition. The SiC and EG reciprocal lattices are related by a well-known 30° epitaxial relationship.[45] If the reciprocal lattice basis vectors $\boldsymbol{a}_{ZnO}$* and $\boldsymbol{a}_{SiC}$* are parallel (as drawn), the Ewald construction in Figure 3c determines that a $\Delta\phi = -17.8°$ rotation of the


dx.doi.org/10.1021/nl4000932 | Nano Lett. XXXX, XXX, XXX−XXX

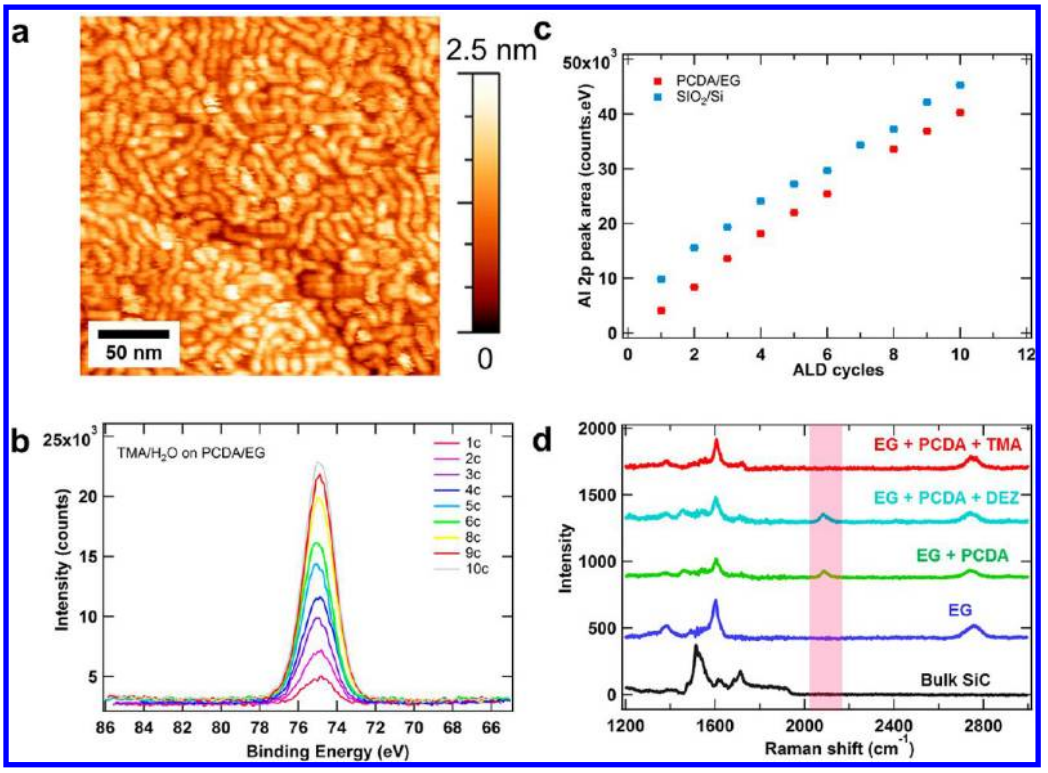


**Figure 4.** (a) AFM image of a PCDA/EG surface after 5 ALD $Al_2O_3$ cycles showing a lamellar morphology. (b) XPS Al 2p peak for PCDA/EG as a function of ALD cycles. The Al 2p position at ~74.7 eV indicates the presence of $Al_2O_3$. The increase in intensity as a function of ALD cycles is attributed to the growth of $Al_2O_3$ with repeated ALD cycles. The spectra were calibrated relative to the C 1s peak at 285 eV. (c) Integrated area of the Al 2p peak as a function of ALD cycles for both PCDA/EG and $SiO_2$/Si. Linear growth with cycle number is seen for both surfaces. (d) Raman spectra of EG, PCDA/EG, ZnO-PCDA/EG, and TMA/$H_2O$ modified PCDA/EG (the bulk SiC spectrum has been subtracted). The peak at 2082 $cm^{-1}$ (highlighted by the pink region) is attributed to the diacetylene stretch of PCDA, which survives DEZ but not TMA ALD chemistry.

sample separates the Bragg condition for the ZnO 1D lattice and the SiC (1 0 *L*) rod. This value agrees well with our measured value of $-18 \pm 0.5°$ (Figure 3b), revealing that the average ZnO chain direction is parallel to the SiC ⟨1 0⟩ family of directions, and therefore the PCDA alkyl tails align along the ⟨1 0⟩ family of directions of the EG lattice. Figure 3d depicts the corresponding real-space representation of the orientational relationships between the EG/SiC, the ZnO-PCDA nanostructure, and the PCDA alkyl chain. In particular, the alkyl tail orientation is consistent with that observed for as-deposited PCDA molecules on HOPG[39] and highlights the effectiveness of PCDA monolayers for templating 1D ALD ZnO nanostructures.

The coordination of Zn to the carboxylic ends of PCDA share features similar to the coordination of divalent metal ions to fatty acids in solution.[46−56] Specifically, divalent metal ions coordinate to the carboxylate groups, with a metal ion to molecule ratio generally believed to be 1:2.[48,54,55,57] Monolayers of these fatty acids coordinated to divalent ions have been deposited from solution or via Langmuir−Blodgett deposition onto a variety of surfaces[52] including HOPG.[57] Similar to that observed for ZnO-PCDA/EG/SiC, the presence of metal ions coordinated to the fatty acids stabilizes the molecules in solution, and enhances the long-range packing order and thermal stability in the resulting monolayer.[52] While the coordination of divalent metal ions to fatty acids in solution is largely believed to be ionic,[46,48,49,53−55] transition metals such as Zn may have multiple carboxylate binding modes, including covalent monodentate and bidentate modes.[58]

In contrast to DEZ, the reaction of trimethyl aluminum (TMA) with PCDA is nonterminating and leads to the growth of $Al_2O_3$ films. ALD $Al_2O_3$ was performed on PCDA/EG substrates by exposure to sequential doses of TMA and $H_2O$. Figure 4b is a plot of the Al 2p XPS peak absolute intensity as a function of ALD cycles. The intensity of the Al 2p XPS peak increases as a function of ALD cycles, which is attributed to the nonterminating reaction of TMA with PCDA and the subsequent growth of $Al_2O_3$. Figure 4c shows the integrated area of the Al 2p peak as function of ALD cycles for both PCDA/EG and $SiO_2$/Si surfaces, which reveal linear ALD growth on both surfaces. Figure 4a is an AFM image of a PCDA/EG surface after 5 cycles of ALD $Al_2O_3$. The resulting disordered lamellar structure is noticeably distinct from the striped morphology of as-deposited PCDA/EG (Figure 1e) and also distinct from the structure after ALD $Al_2O_3$ deposition on bare graphene (Figure S5, Supporting Information), which shows discontinuous film growth.[14,21]

Raman spectroscopy was employed to determine the chemical activity of the PCDA monolayer following ALD oxide deposition as shown in Figure 4d. The acetylene stretching frequency for PCDA is located between 2077 $cm^{-1}$ and 2101 $cm^{-1}$, depending on the degree of polymerization and side chain disorder.[59−61] Raman spectra for PCDA on EG show peaks due to the graphene phonons (D band at 1380 $cm^{-1}$, G band at 1604 $cm^{-1}$, and 2D band at 2742 $cm^{-1}$), the PCDA acetylene stretch centered at 2082 $cm^{-1}$, and a peak at 1458 $cm^{-1}$ attributed to a C═C stretch. First, the breadth and asymmetry of the acetylene stretch of as-deposited PCDA/EG indicate that there could be a coexistence of the "blue" and


dx.doi.org/10.1021/nl4000932 | *Nano Lett.* XXXX, XXX, XXX−XXX

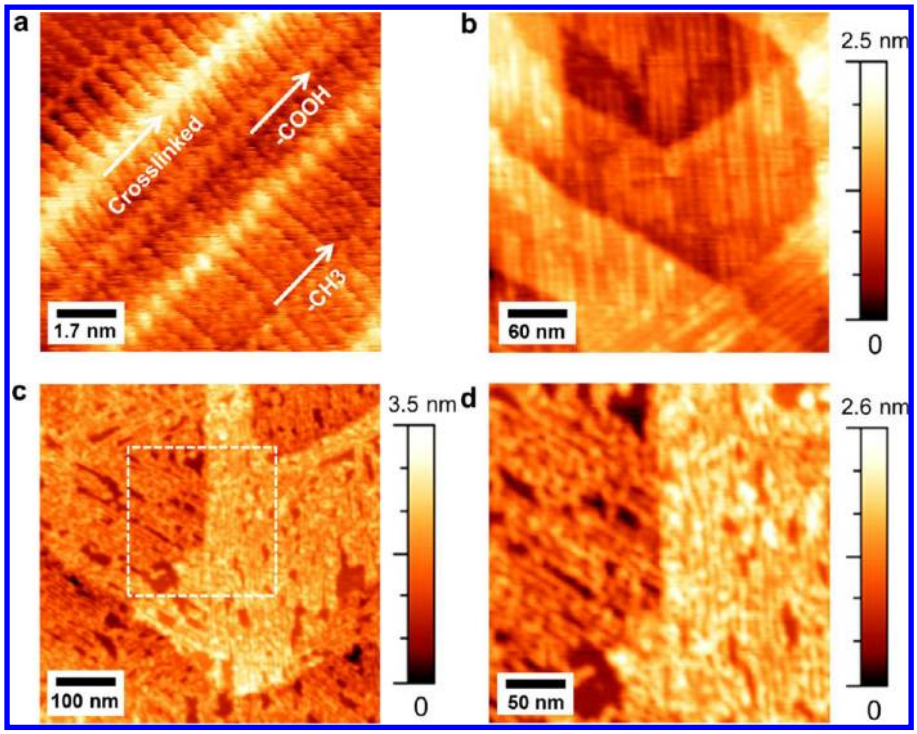


**Figure 5.** Atomic layer deposition on cross-linked PCDA/EG. (a) Molecularly resolved UHV STM image showing the cross-linked diacetylene cores of PCDA next to a molecular chain that has not yet undergone cross-linking. (b) AFM image in ambient of a UV irradiated PCDA/EG surface showing the presence of elevated stripes attributed to cross-linked PCDA. (c) AFM image after 5 ALD $Al_2O_3$ cycles on cross-linked PCDA/EG. (d) Zoomed-in image of part c, showing better aligned arrays compared to $Al_2O_3$ on as-deposited PCDA/EG (Figure 4a). The UV irradiation time was 90 min.

"red" polymer PCDA phases on the graphene surface, which are nominally attributed to an ordered and disordered polymer, respectively,[59−61] which is also corroborated by the C═C stretch[59] present in the "blue phase". The presence of these polymer phases indicates that some polymerization of PCDA is occurring under Raman laser irradiation.

Following ALD of zinc oxide using DEZ and water, the acetylene peak remains and shifts to a slightly higher frequency (2087 $cm^{-1}$), and the C═C stretch remains at 1458 $cm^{-1}$. The persistence of these stretches with the same spectral intensity as in the neat PCDA film reveals that the DEZ does not interact with the acetylene carbons. In contrast, deposition of alumina via TMA and $H_2O$ destroys the vibrations of both the acetylene and C═C stretch, thus pointing to the loss of these functional groups due to attack by the more aggressive TMA precursor. Furthermore, it is observed that an initially striped ZnO-PCDA/EG surface is transformed to the disordered lamellar structure upon TMA and $H_2O$ exposures as seen in Figure S6, Supporting Information.

While TMA is expected to react with the carboxylate group of PCDA according to previous work on nonhydrolytic ALD with carboxylic acids,[62−64] Raman spectroscopy indicates that TMA additionally attacks the acetylene groups. This attack by TMA share similarities with carboalumination reactions, which can involve the reaction of aluminum alkyls with carbon−carbon double and triple bonds, and is a well-established synthetic protocol in organometallic chemistry and organic synthesis (e.g., Ziegler−Natta polymerization).[65−68]

Since the acetylene groups are a primary contributor to PCDA monolayer stability and are subject to attack by TMA, cross-linking the PCDA preceding ALD is likely to enhance the ordering stability during $Al_2O_3$ deposition. To test this hypothesis, cross-linking of PCDA was performed on EG via ultraviolet (UV) irradiation.[38] In particular, PCDA/EG substrates were exposed to UV irradiation from a UV pen lamp (254 nm, Spectroline, 11SC-1) in a $N_2$ glovebox. The cross-linked diacetylene cores of PCDA molecules are shown in the molecularly resolved STM image of Figure 5a. The mechanism of UV polymerization, the changes in the angle of the side chains, and the height of the polymerized PCDA chains on EG have been reported previously.[38] An AFM image of a PCDA/EG surface after a 90 min UV irradiation is shown in Figure 5b, revealing elevated stripes, ∼2.5 Å high, that are attributed to the polymerized PCDA chains.[38] The spatial extent of cross-linking can be modulated by the UV irradiation time as shown in Figure S7, Supporting Information.

Parts c and d of Figure 5 are AFM images after five $Al_2O_3$ ALD cycles on a 90 min UV irradiated PCDA/EG sample. The presence of aligned stripes and sharp edges in contrast to the lamellar structure observed on as-deposited PCDA (Figure 4a), indicate that cross-linking enhances ordering following $Al_2O_3$ ALD. This improved ordering can be attributed to the enhanced structural and thermal stability provided by cross-linking as demonstrated by desorption measurements in Figure S8, Supporting Information. Lateral growth of $Al_2O_3$ on PCDA is observed with increasing number of ALD cycles as shown in Figure S9, Supporting Information. In this case, the thicker $Al_2O_3$ films continue to possess sharp and aligned edges, templated by the underlying monolayer, although the top-surface becomes nonuniform.

In summary, self-assembled organic monolayers of PCDA have been used as a template for directed ALD growth on EG/SiC(0001). UHV-sublimated PCDA self-assembles into well-ordered monolayer domains consisting of one-dimensional


dx.doi.org/10.1021/nl4000932 | *Nano Lett.* XXXX, XXX, XXX−XXX

molecular arrays that coat the surface in a manner consistent with the symmetry of the underlying graphene lattice. Diethyl zinc (DEZ) and trimethyl aluminum (TMA), typical ALD chemistries for the growth of ZnO and $Al_2O_3$, respectively, were investigated on these PCDA/EG templates. DEZ was found to react with PCDA/EG in a self-terminating manner, where the original striped morphology of PCDA was retained following exposure. Furthermore, DEZ treatment enhances the thermal stability of PCDA/EG, which subsequently promotes enhanced ordering as the maximum domain size increases by a factor of 4 compared to unmodified PCDA/EG following annealing. Spectroscopic and X-ray scattering experiments suggest that DEZ reacts with the carboxylate groups of PCDA, where Zn atoms coordinate between neighboring PCDA molecules. Furthermore, due to this templating effect, the ZnO chains are shown to align only along specific orientations with respect to the underlying graphene lattice. On the other hand, sequential exposures of PCDA to TMA/$H_2O$ lead to the nonterminating ALD growth of $Al_2O_3$. In contrast to the as-deposited PCDA/EG surface, $Al_2O_3$ growth on PCDA/EG results in a disordered lamellar morphology, due in part to the absence of the stabilizing PCDA acetylene groups, which are attacked and removed by TMA exposure. Finally, cross-linking PCDA via UV irradiation enhances its stability, allowing for the ordered vertical growth of $Al_2O_3$, up to five TMA/$H_2O$ ALD cycles, before lateral $Al_2O_3$ growth outside of the template becomes dominant. Overall, the combination of PCDA and ALD provides multiple pathways to forming sub-10 nm oxide nanostructures on graphene, which can likely benefit ongoing efforts to realize graphene-based nanoelectronic, sensing, and energy technologies.

## ■ ASSOCIATED CONTENT

### Supporting Information

Detailed experimental methods and materials, enhancement of thermal properties of PCDA by DEZ modification, large domain formations of DEZ modified PCDA, X-ray scattering data, STM analysis of PCDA structure and orientation on EG/SiC, ALD $Al_2O_3$ on bare graphene, effect of TMA on ZnO-PCDA ordering, UV irradiation of PCDA, influence of cross-linking on thermal properties of PCDA, and lateral growth of $Al_2O_3$ on cross-linked PCDA. This material is available free of charge via the Internet at http://pubs.acs.org.

## ■ AUTHOR INFORMATION


### Corresponding Author

*Telephone: (847) 491- 2696. Fax: (847) 491- 7820. E-mail: m-hersam@northwestern.edu.

### Present Address

#Current address: Indian Institute of Science Education and Research, Pashan, Pune 411021, India.


### Author Contributions

The manuscript was written through contributions of all authors. All authors have given approval to the final version of the manuscript.

### Notes

The authors declare no competing financial interest.

## ■ ACKNOWLEDGMENTS

This work was supported by the Office of Naval Research (Award Numbers N00014-11-1-0463), Air Force Office of Scientific Research (FA9550-11-1-0275), Department of Energy (Award Number DE-FG02-09ER16109), Northwestern Materials Research Science and Engineering Center (NSF Award Number DMR-1121262), and Argonne National Laboratory (ANL). ANL is a U.S. Department of Energy Office of Science Laboratory operated under Contract No. DE-AC02-06CH11357 by UChicago Argonne, LLC. J.M.P.A. and M.C.H. acknowledge an IBM Ph.D. Fellowship and W. M. Keck Foundation Science and Engineering Grant, respectively. This work made use of the NUANCE and J.B. Cohen X-ray facilities at Northwestern University, which are supported by the NSF-NSEC, NSF-MRSEC, Keck Foundation, and State of Illinois. Use of the Advanced Photon Source, 8-ID-E beamline was supported under the ANL contract listed above. We would like to acknowledge Joe Strzalka (APS Sector 8) for beamline support and assistance with experimental design.

## ■ REFERENCES


(1) Castro Neto, A. H.; Guinea, F.; Peres, N. M. R.; Novoselov, K. S.; Geim, A. K. *Rev. Mod. Phys.* **2009**, *81*, 109−162.

(2) Geim, A. K.; Novoselov, K. S. *Nat. Mater.* **2007**, *6*, 183−191.

(3) Farmer, D. B.; Chiu, H. Y.; Lin, Y. M.; Jenkins, K. A.; Xia, F. N.; Avouris, P. *Nano Lett.* **2009**, *9*, 4474−4478.

(4) Lin, Y. M.; Dimitrakopoulos, C.; Jenkins, K. A.; Farmer, D. B.; Chiu, H. Y.; Grill, A.; Avouris, P. *Science* **2010**, *327*, 662−662.

(5) Lin, Y. M.; Jenkins, K. A.; Valdes-Garcia, A.; Small, J. P.; Farmer, D. B.; Avouris, P. *Nano Lett.* **2009**, *9*, 422−426.

(6) Avouris, P. *Nano Lett.* **2010**, *10*, 4285−4294.

(7) Schedin, F.; Geim, A. K.; Morozov, S. V.; Hill, E. W.; Blake, P.; Katsnelson, M. I.; Novoselov, K. S. *Nat. Mater.* **2007**, *6*, 652−655.

(8) Geim, A. K. *Science* **2009**, *324*, 1530−1534.

(9) Wang, Q. H.; Hersam, M. C. *MRS Bull.* **2011**, *36*, 532−542.

(10) Hossain, M. Z.; Johns, J. E.; Bevan, K. H.; Karmel, H. J.; Liang, Y. T.; Yoshimoto, S.; Mukai, K.; Koitaya, T.; Yoshinobu, J.; Kawai, M.; Lear, A. M.; Kesmodel, L. L.; Tait, S. L.; Hersam, M. C. *Nat Chem.* **2012**, *4*, 305−309.

(11) Hossain, M. Z.; Walsh, M. A.; Hersam, M. C. *J. Am. Chem. Soc.* **2010**, *132*, 15399−15403.

(12) Hummers, W. S.; Offeman, R. E. *J. Am. Chem. Soc.* **1958**, *80*, 1339−1339.

(13) Dreyer, D. R.; Park, S.; Bielawski, C. W.; Ruoff, R. S. *Chem. Soc. Rev.* **2010**, *39*, 228−240.

(14) Alaboson, J. M. P.; Wang, Q. H.; Emery, J. D.; Lipson, A. L.; Bedzyk, M. J.; Elam, J. W.; Pellin, M. J.; Hersam, M. C. *ACS Nano* **2011**, *5*, 5223−5232.

(15) Wang, Q. H.; Hersam, M. C. *Nat. Chem.* **2009**, *1*, 206−211.

(16) Sinitskii, A.; Tour, J. M. *J. Am. Chem. Soc.* **2010**, *132*, 14730−14732.

(17) Jandhyala, S.; Mordi, G.; Lee, B.; Lee, G.; Floresca, C.; Cha, P. R.; Ahn, J.; Wallace, R. M.; Chabal, Y. J.; Kim, M. J.; Colombo, L.; Cho, K.; Kim, J. *ACS Nano* **2012**, *6*, 2722−2730.

(18) Lee, B.; Mordi, G.; Kim, M. J.; Chabal, Y. J.; Vogel, E. M.; Wallace, R. M.; Cho, K. J.; Colombo, L.; Kim, J. *Appl. Phys. Lett.* **2010**, *97*, 043107.

(19) Shen, T.; Gu, J. J.; Xu, M.; Wu, Y. Q.; Bolen, M. L.; Capano, M. A.; Engel, L. W.; Ye, P. D. *Appl. Phys. Lett.* **2009**, *95*, 172105.

(20) Kim, S.; Nah, J.; Jo, I.; Shahrjerdi, D.; Colombo, L.; Yao, Z.; Tutuc, E.; Banerjee, S. K. *Appl. Phys. Lett.* **2009**, *94*, 062107.

(21) Wang, X. R.; Tabakman, S. M.; Dai, H. J. *J. Am. Chem. Soc.* **2008**, *130*, 8152−8153.

(22) Green, A. A.; Hersam, M. C. *Nano Lett.* **2009**, *9*, 4031−4036.

(23) Green, A. A.; Hersam, M. C. *J. Phys. Chem. Lett.* **2010**, *1*, 544−549.

(24) Li, D.; Muller, M. B.; Gilje, S.; Kaner, R. B.; Wallace, G. G. *Nat. Nanotechnol.* **2008**, *3*, 101−105.

(25) Si, Y.; Samulski, E. T. *Nano Lett.* **2008**, *8*, 1679−1682.

(26) Stankovich, S.; Dikin, D. A.; Dommett, G. H. B.; Kohlhaas, K. M.; Zimney, E. J.; Stach, E. A.; Piner, R. D.; Nguyen, S. T.; Ruoff, R. S. *Nature* **2006**, *442*, 282−286.
(27) Ramanathan, T.; Abdala, A. A.; Stankovich, S.; Dikin, D. A.; Herrera-Alonso, M.; Piner, R. D.; Adamson, D. H.; Schniepp, H. C.; Chen, X.; Ruoff, R. S.; Nguyen, S. T.; Aksay, I. A.; Prud'homme, R. K.; Brinson, L. C. *Nat. Nanotechnol.* **2008**, *3*, 327−331.
(28) Kim, H.; Abdala, A. A.; Macosko, C. W. *Macromolecules* **2010**, *43*, 6515−6530.
(29) Liang, Y. T.; Hersam, M. C. *Macromol. Chem. Phys.* **2012**, *213*, 1091−1100.
(30) Wang, Q. H.; Hersam, M. C. *Nano Lett.* **2011**, *11*, 589−593.
(31) Alaboson, J. M. P.; Wang, Q. H.; Kellar, J. A.; Park, J.; Elam, J. W.; Pellin, M. J.; Hersam, M. C. *Adv. Mater.* **2011**, *23*, 2181−2184.
(32) Byun, I. S.; Yoon, D.; Choi, J. S.; Hwang, I.; Lee, D. H.; Lee, M. J.; Kawai, T.; Son, Y. W.; Jia, Q.; Cheong, H.; Park, B. H. *ACS Nano* **2011**, *5*, 6417−6424.
(33) Kim, M.; Safron, N. S.; Han, E.; Arnold, M. S.; Gopalan, P. *Nano Lett.* **2010**, *10*, 1125−1131.
(34) Prado, M. C.; Nascimento, R.; Moura, L. G.; Matos, M. J. S.; Mazzoni, M. S. C.; Cancado, L. G.; Chacham, H.; Neves, B. R. A. *ACS Nano* **2011**, *5*, 394−398.
(35) Kim, S. S.; Choi, J. Y.; Kim, K.; Sohn, B. H. *Nanotechnology* **2012**, *23*, 125301.
(36) Bai, J. W.; Zhong, X.; Jiang, S.; Huang, Y.; Duan, X. F. *Nat. Nanotechnol.* **2010**, *5*, 190−194.
(37) Liu, L.; Zhang, Y. L.; Wang, W. L.; Gu, C. Z.; Bai, X. D.; Wang, E. G. *Adv. Mater.* **2011**, *23*, 1246−1251.
(38) Deshpande, A.; Sham, C. H.; Alaboson, J. M.; Mullin, J. M.; Schatz, G. C.; Hersam, M. C. *J. Am. Chem. Soc.* **2012**, *134*, 16759−16764.
(39) Okawa, Y.; Takajo, D.; Tsukamoto, S.; Hasegawa, T.; Aono, M. *Soft Mater.* **2008**, *4*, 1041−1047.
(40) Okawa, Y.; Aono, M. *J. Chem. Phys.* **2001**, *115*, 2317−2322.
(41) Giridharagopal, R.; Kelly, K. F. *ACS Nano* **2008**, *2*, 1571−1580.
(42) Elam, J. W.; Groner, M. D.; George, S. M. *Rev. Sci. Instrum.* **2002**, *73*, 2981−2987.
(43) George, S. M.; Ott, A. W.; Klaus, J. W. *J. Phys. Chem.* **1996**, *100*, 13121−13131.
(44) Fontes, G. N.; Neves, B. R. A. *Langmuir* **2005**, *21*, 11113−11118.
(45) van Bommel, A. J.; Crombeen, J. E.; Vantooren, A. *Surf. Sci.* **1975**, *48*, 463−472.
(46) Spink, J. A.; Sanders, J. V. *T. Faraday Soc.* **1955**, *51*, 1154−1165.
(47) Neuman, R. D. *J. Colloid Interface Sci.* **1975**, *53*, 161−171.
(48) June, D.; Franses, E. I. *J. Chem. Phys.* **1991**, *95*, 8486−8493.
(49) Binks, B. P. *Adv. Colloid Interfac.* **1991**, *34*, 343−432.
(50) Linden, D. J. M.; Peltonen, J. P. K.; Rosenholm, J. B. *Langmuir* **1994**, *10*, 1592−1595.
(51) Li, H. H.; Mao, G. Z.; Ng, K. Y. S. *Thin Solid Films* **2000**, *358*, 62−72.
(52) Schwartz, D. K.; Garnaes, J.; Viswanathan, R.; Zasadzinski, J. A. N. *Science* **1992**, *257*, 508−511.
(53) Bloch, J. M.; Yun, W. B. *Phys. Rev. A* **1990**, *41*, 844−862.
(54) Elliot, D. J.; Furlong, D. N.; Grieser, F. *Colloid Surf. A* **1998**, *141*, 9−17.
(55) Matsuura, N.; Elliot, D. J.; Furlong, D. N.; Grieser, F. *Colloid Surf. A* **1997**, *126*, 189−195.
(56) Kundu, S.; Datta, A.; Hazra, S. *Chem. Phys. Lett.* **2005**, *405*, 282−287.
(57) Mao, G. Z.; Dong, W. F.; Kurth, D. G.; Mohwald, H. *Nano Lett.* **2004**, *4*, 249−252.
(58) Zelenak, V.; Vargova, Z.; Gyoryova, K. *Spectrochim. Acta A* **2007**, *66*, 262−272.
(59) Joo, S. W.; Lim, J. K.; Cho, K. *J. Photochem. Photobiol. A* **2008**, *194*, 356−361.
(60) Lifshitz, Y.; Upcher, A.; Shusterman, O.; Horovitz, B.; Berman, A.; Golan, Y. *Phys. Chem. Chem. Phys.* **2010**, *12*, 713−722.
(61) Cai, M.; Mowery, M. D.; Pemberton, J. E.; Evans, C. E. *Appl. Spectrosc.* **2000**, *54*, 31−38.
(62) Li, M.; Dai, M.; Chabal, Y. J. *Langmuir* **2009**, *25*, 1911−1914.
(63) Klepper, K. B.; Nilsen, O.; Fjellvag, H. *Dalton T.* **2010**, *39*, 11628−11635.
(64) Yoon, B.; Seghete, D.; Cavanagh, A. S.; George, S. M. *Chem. Mater.* **2009**, *21*, 5365−5374.
(65) Fallis, A. G.; Forgione, P. *Tetrahedron* **2001**, *57*, 5899−5913.
(66) Wipf, P.; Lim, S. *Angew. Chem., Int. Ed.* **1993**, *32*, 1068−1071.
(67) Egger, K. W.; Cocks, A. T. *J. Am. Chem. Soc.* **1972**, *94*, 1810−1815.
(68) Bundens, J. W.; Yudenfreund, J.; Francl, M. M. *Organometallics* **1999**, *18*, 3913−3920.